Space-time PML and Subgrid Connections for Finite Integration Method

Kota Arai, Takeshi Mifune, *Member, IEEE,* Tetsuji Matsuo, *Member, IEEE*

Graduate School of Engineering, Kyoto University, Kyoto 615-8510, Japan, araikota@fem.kuee.kyoto-u.ac.jp

The perfectly matched layer (PML) absorbing boundary is employed in the space-time finite integration (FI) method. Subgrid connections in 3D and 4D space-time are considered. Using the PML, the computational accuracy for 3D and 4D space-time subgrid methods are evaluated. The subgrid scheme given by the space-time FI method suppresses unphysical wave reflections compared with the subgrid scheme based on the spatial FI method.

***Index Terms*— Boundary condition, electromagnetic wave absorption, finite integration method, time-domain analysis.**

I. Introduction

The electromagnetic field analysis of fine structure at sub-wavelength scales is required for advanced electronic and optical devices [1]. The analysis of these devices using the conventional FDTD method [2] incurs large computational cost because the spatial grid should be refined uniformly unless a sophisticated subgrid method [2] is used for an adaptive grid construction.

The finite integration (FI) method [3]–[5] is an alternative choice for time-domain analysis using a spatial adaptive grid that produces a stable subgrid scheme [6]. The space-time FI method [7], [8] is an advanced version of the FI method that enables efficient electromagnetic field computations using an adaptive time-step. Ref. [9] proposed 3D and 4D space-time subgrid methods for the adaptive grid construction and provided comparisons with the spatial FI subgrid scheme [6]. However, the computational accuracy of the space-time subgrid scheme has not as yet been fully examined because only periodic spatial boundary conditions were implemented.

This paper develops the connection scheme to the perfectly matched layer (PML) [10] for the space-time FI method and discusses the 3D and 4D connections to space-time subgrids constructing the Hodge dual grid [7].

II. Space-time finite integration method

Points in the coordinate system are denoted by (w, x, y, z) = (x^0, x^1, x^2, x^3) where $w = ct$, $c = 1/\sqrt{\varepsilon_0\mu_0}$, and ε_0 and μ_0 are the permittivity and permeability of vacuum, respectively. The integral form of the Maxwell equations [7] is given as

$$\oint_{\partial\Omega_p} F = 0, \oint_{\partial\Omega_d} G = \int_{\Omega_d} J \tag{1}$$

$$F = -\sum_{i=1}^{3} E_i \mathrm{d}x^0 \mathrm{d}x^i + \sum_{j=1}^{3} cB_j \mathrm{d}x^k \mathrm{d}x^l , \tag{2}$$

$$G = \sum_{i=1}^{3} H_i \mathrm{d}x^0 \mathrm{d}x^i + \sum_{j=1}^{3} cD_j \mathrm{d}x^k \mathrm{d}x^l , \tag{3}$$

$$J = \mathrm{c}\rho dx^1 dx^2 dx^3 - \sum_{j=1}^{3} J_j \mathrm{d}x^0 \mathrm{d}x^k \mathrm{d}x^l , \tag{4}$$

where (j, k, l) is a cyclic permutation of $(1, 2, 3)$, and Ω_p and Ω_d are hypersurfaces in space-time; $\partial\Omega_p$ and $\partial\Omega_d$ denote the faces of the primal and dual grids, respectively; ρ is the electric charge density and J_j is the electric current density. The electromagnetic variables in the FI method are defined as

$$f = \int_{S_p} F , g = \int_{S_d} G, \tag{5}$$

where S_p and S_d are the faces of the primal and dual grids $\partial\Omega_p$ and $\partial\Omega_d$. To express the constitutive equation simply, the Hodge dual grid [7] is introduced as

$$\frac{\int_{Sd} c_r \mathrm{d}x^0 \mathrm{d}x^j}{\int_{Sp} \mathrm{d}x^k \mathrm{d}x^l} = -\frac{\int_{Sd} \mathrm{d}x^k \mathrm{d}x^l}{\int_{Sp} c_r \mathrm{d}x^0 \mathrm{d}x^j} = \kappa , \tag{6}$$

where $c_r = 1/\sqrt{\varepsilon_r\mu_r}$; κ is a constant determined for each pair of S_p and S_d; and ε_r and μ_r are the relative permittivity and permeability, respectively. From (5) and (6), it follows that $f = Zg/\kappa$, where $Z = \sqrt{\mu_r\mu_0/(\varepsilon_r\varepsilon_0)}$ is the impedance. A systematic formulation of the space-time FI method using incidence matrices is presented in [8].

III. PML absorbing boundary condition

In the 3D space, all the components of the electric flux density and the magnetic flux density are divided into two subcomponents respectively such that

$$D_x = D_{xy} + D_{xz}, \tag{7}$$

where D_{xy} and D_{xz} are the respective components of D_x propagating along the y and z-directions. Using these subcomponents, the space-time FI method updates the electric flux density in the PML as

$$\begin{aligned} d_{xy,i-\frac{1}{2},j-\frac{1}{2},k-\frac{1}{2}}^{\;n+\frac{1}{2}} &= \frac{1-\frac{\Delta w}{2}\sigma_y Z}{1+\frac{\Delta w}{2}\sigma_y Z} d_{xy,\,i-\frac{1}{2},j-\frac{1}{2},k-\frac{1}{2}}^{\;n-\frac{1}{2}} \\ &+ \frac{1}{1+\frac{\Delta w}{2}\sigma_y Z}\left(h_{z,\,i-\frac{1}{2},j,k-\frac{1}{2}}^{\;n} - h_{z,\,i-\frac{1}{2},j-1,k-\frac{1}{2}}^{\;n}\right), \\ d_{xz,i-\frac{1}{2},j-\frac{1}{2},k-\frac{1}{2}}^{\;n+\frac{1}{2}} &= \frac{1-\frac{\Delta w}{2}\sigma_z Z}{1+\frac{\Delta w}{2}\sigma_z Z} d_{xz,\,i-\frac{1}{2},j-\frac{1}{2},k-\frac{1}{2}}^{\;n-\frac{1}{2}} \\ &- \frac{1}{1+\frac{\Delta w}{2}\sigma_z Z}\left(h_{y,\,i-\frac{1}{2},j-\frac{1}{2},k}^{\;n} - h_{y,\,i-\frac{1}{2},j-\frac{1}{2},k-1}^{\;n}\right), \end{aligned} \tag{8}$$

Manuscript received April 1, 2015; revised May 15, 2015 and June 1, 2015; accepted July 1, 2015. Date of publication July 10, 2015; date of current version July 31, 2015. Corresponding author: T. Matsuo (e-mail: matsuo.tetsuji.5u@kyoto-u.ac.jp).

Color versions of one or more of the figures in this paper are available online at http://ieeexplore.ieee.org.

Digital Object Identifier (inserted by IEEE).

where σ_y and σ_z are the electric conductivities in the y and z-directions, respectively, Δw is the time-step, the subscripts are spatial indices for the x, y, and z directions, and the superscript is the temporal index. The time-marching scheme for the other variables is given similarly.

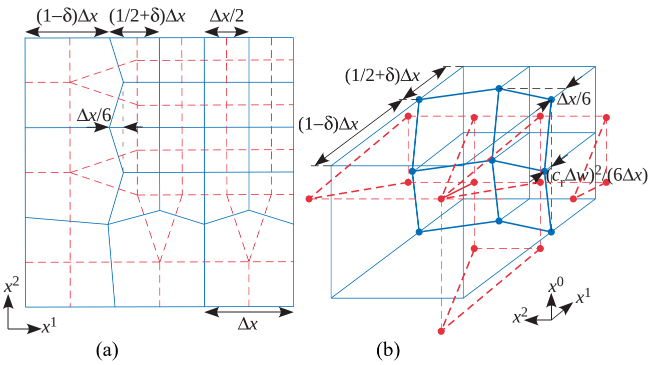

Fig. 1. 3D space-time subgrid of straight type: (a) corner part and (b) space-time connection.

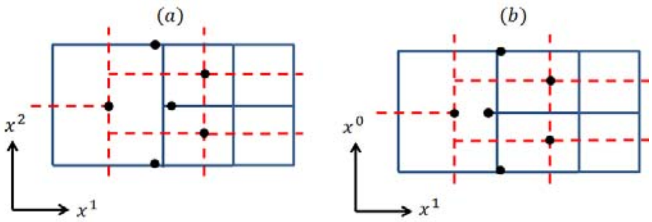

Fig. 2. 3D space-time subgrid of staircase type: (a) spatial and (b) space-time connections.

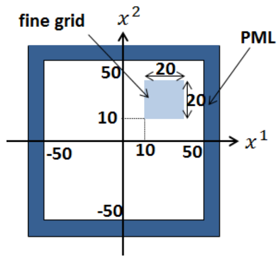

Fig. 3. Computational domain showing subgrid and PML.

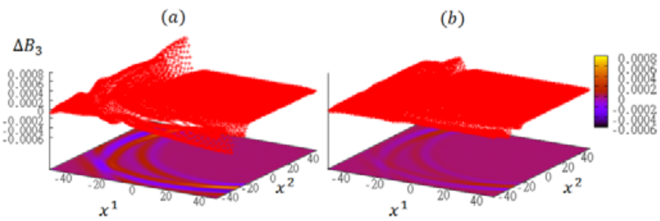

Fig. 4. Discrepancy of B_3 compared with FDTD method: (a) δ=0.01 and (b) δ=0.1.

IV. Space-Time Subgrid Connection

Ref. [9] proposed straight-type and staircase-type subgrids in the 3D and 4D space-times. However, the subgrid connection in 4D space-time was not discussed in detail because the 4D geometry is not always intuitively explainable. This section gives an explicit description of the connecting faces at the subgrid boundary.

A. 3D space-time subgrid

The 3D straight-type and staircase-type space-time subgrids are examined with the PML boundary condition. Fig. 1 illustrates the straight-type subgrid connection, where δ is a free parameter to locate the subgrid boundary. Ref. [9] proposed the staircase-type subgrid connection (Fig. 2) bending the edges and faces of the space-time grid.

Fig. 3 illustrates the computational domain having the subgrid and PML. For simplicity, the permittivity and permeability are set uniformly to unity by the normalization replacing the variable F by $F/\sqrt{\mu_0/\varepsilon_0}$. The coordinates are linearly transformed to normalize Δx to 1; the normalized temporal step Δw is set to 0.5. The normalized initial conditions are $E_1 = E_2 = 0$ and $B_3 = \exp\{-[(x^1)^2+(x^2)^2]/25\}$. Fig. 4 depicts the distributions of discrepancy ΔB_3 between B_3 obtained employing the FDTD method and that obtained using the 3D staircase-type space-time subgrid at ct = 100 with δ=0.01 and 0.1. Unphysical wave reflection caused by the subgrid connection is reduced by the optimization of δ.

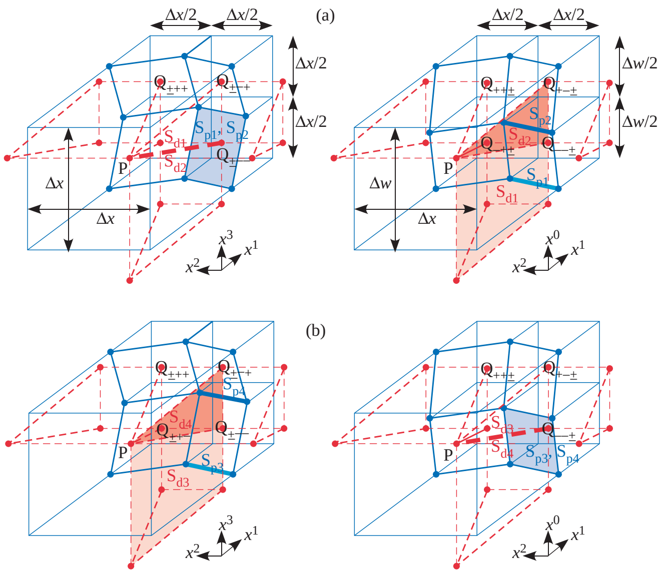

Fig. 5. 4D straight-type subgrid connection: (a) faces S_{p1}, S_{p2}, S_{d1}, S_{d2}, and (b) faces S_{p3}, S_{p4}, S_{d3}, S_{d4}.

B. 4D Straight-type subgrid

We use bases dx_i satisfying $dx^k dx_i = \delta^k_i$ to represent edges and $dx_i \wedge dx_j$ to represent faces having subscripts i, j = 0, 1, 2, 3, where ∧ denotes the wedge product.

Fig. 5 illustrates the straight-type subgrid connection, where eight edges connect the node P: (0, 0, 0, 0) on the coarse grid side and the eight nodes $Q_{\pm\pm\pm}$: ($\pm\Delta w/4$, $3\Delta x/4$, $\pm\Delta x/4$, $\pm\Delta x/4$) on the fine grid side of dual grid. The edge to node Q_{---} from P is represented as $\Delta x(3dx_1/4 - dx_2/4 - dx_3/4) - \Delta w dx_0/4$. This edge belongs to the faces S_{di} (i = 1, …, 4) of the dual grid, which are represented as

$$S_{d1} = \frac{3\Delta w}{4} dx_0 \wedge \left[\Delta x\left(\frac{3}{4}dx_1 - \frac{1}{4}dx_2 - \frac{1}{4}dx_3\right) - \frac{\Delta w}{4}dx_0\right],$$

$$S_{d2} = \frac{\Delta w}{4} dx_0 \wedge \left[\Delta x\left(\frac{3}{4}dx_1 - \frac{1}{4}dx_2 - \frac{1}{4}dx_3\right) - \frac{\Delta w}{4}dx_0\right]. \quad (9)$$

$$S_{d3} = \left[\Delta x\left(\frac{3}{4}\mathrm{d}x_1 - \frac{1}{4}\mathrm{d}x_2 - \frac{1}{4}\mathrm{d}x_3\right) - \frac{\Delta w}{4}\mathrm{d}x_0\right] \wedge \frac{3\Delta x}{4}\mathrm{d}x_3,$$
$$S_{d4} = \left[\Delta x\left(\frac{3}{4}\mathrm{d}x_1 - \frac{1}{4}\mathrm{d}x_2 - \frac{1}{4}\mathrm{d}x_3\right) - \frac{\Delta w}{4}\mathrm{d}x_0\right] \wedge \frac{\Delta x}{4}\mathrm{d}x_3. \qquad (10)$$

Based on (6), the corresponding faces S_{pi} (i = 1,…,4) of the primal grid are slanted:

$$S_{p1} = S_{p2} = \Delta x\left(\frac{1}{2}\mathrm{d}x_2 + \frac{1}{6}\mathrm{d}x_1\right) \wedge \Delta x\left(\frac{1}{2}\mathrm{d}x_3 + \frac{1}{6}\mathrm{d}x_1\right) \qquad (11)$$

$$S_{p3} = S_{p4} = \left[\frac{\Delta w}{2}\mathrm{d}x_0 - \frac{(c_\mathrm{r}\Delta w)^2}{6\Delta x}\mathrm{d}x_1\right] \wedge \Delta x\left(\frac{1}{2}\mathrm{d}x_2 + \frac{1}{6}\mathrm{d}x_1\right). \qquad (12)$$

Of the variables $f_i = \int_{Spi}F$ and $g_i = \int_{Sdi}G$ (i = 1,…,4), f_1 and f_2 denote the magnetic fluxes whereas g_1 and g_2 are the magnetomotive forces with

$$f_1 = (\Delta x)^2\frac{3cB_1 - cB_2 - cB_3}{12}, \qquad (13)$$

$$g_1 = 3\Delta x\Delta w\frac{3H_1 - H_2 - H_3}{16} = \frac{9c_\mathrm{r}\Delta w f_1}{4\Delta x Z}. \qquad (14)$$

The dominant component of f_3 and f_4 is the electromotive force but also contain magnetic fluxes such that

$$f_3 = \Delta w\frac{-\Delta x(3E_2 + E_1) - \Delta w c_\mathrm{r}^2 cB_3}{12}. \qquad (15)$$

Similarly, the dominant component of g_3 and g_4 is the electric flux but g_3 and g_4 also include a magnetomotive force dependence such that

$$g_3 = 3\Delta x\frac{-\Delta x(3cD_2 + cD_1) - \Delta w H_3}{16} = \frac{9\Delta x f_3}{4c_\mathrm{r}Z\Delta w}. \qquad (16)$$

C. *4D Staircase type subgrid*

Fig.6 illustrates the staircase-type subgrid connection, where the edges from node P to nodes $Q_{\pm\pm\pm}$ are bent at the points $R_{\pm\pm\pm}$: (±Δw/4, 0, ±Δx/4, ±Δx/4). Consequently, the face S_{d1} has different direction from S_{d2} as

$$S_{d1} = \Delta x\Delta w\left(\frac{3}{8}\mathrm{d}x_0\mathrm{d}x_1 - \frac{3}{16}\mathrm{d}x_0\mathrm{d}x_2 - \frac{3}{16}\mathrm{d}x_0\mathrm{d}x_3\right),$$
$$S_{d2} = \Delta x\Delta w\left(\frac{3}{8}\mathrm{d}x_0\mathrm{d}x_1 - \frac{1}{16}\mathrm{d}x_0\mathrm{d}x_2 - \frac{1}{16}\mathrm{d}x_0\mathrm{d}x_3\right). \qquad (17)$$

The face S_{d3} also has a different direction from S_{d4},

$$S_{d3} = (\Delta x)^2\left(-\frac{3}{8}\mathrm{d}x_3\mathrm{d}x_1 - \frac{3}{16}\mathrm{d}x_2\mathrm{d}x_3\right) - \frac{3\Delta x\Delta w}{16}\mathrm{d}x_0\mathrm{d}x_3,$$
$$S_{d4} = (\Delta x)^2\left(-\frac{3}{8}\mathrm{d}x_3\mathrm{d}x_1 - \frac{1}{16}\mathrm{d}x_2\mathrm{d}x_3\right) - \frac{\Delta x\Delta w}{16}\mathrm{d}x_0\mathrm{d}x_3. \qquad (18)$$

Based on (6), the corresponding faces S_{pi} (i = 1, …, 4) are slanted:

$$S_{p1} = (\Delta x)^2\left(\frac{1}{4}\mathrm{d}x_2\mathrm{d}x_3 - \frac{1}{8}\mathrm{d}x_3\mathrm{d}x_1 - \frac{1}{8}\mathrm{d}x_1\mathrm{d}x_2\right),$$
$$S_{p2} = (\Delta x)^2\left(\frac{1}{4}\mathrm{d}x_2\mathrm{d}x_3 - \frac{1}{24}\mathrm{d}x_3\mathrm{d}x_0 - \frac{1}{24}\mathrm{d}x_1\mathrm{d}x_2\right), \qquad (19)$$
$$S_{p3} = \Delta x\Delta w\left(\frac{1}{4}\mathrm{d}x_0\mathrm{d}x_2 + \frac{1}{8}\mathrm{d}x_0\mathrm{d}x_1\right) - (c_\mathrm{r}\Delta w)^2\frac{1}{8}\mathrm{d}x_1\mathrm{d}x_2,$$
$$S_{p4} = \Delta x\Delta w\left(\frac{1}{4}\mathrm{d}x_0\mathrm{d}x_2 + \frac{1}{24}\mathrm{d}x_0\mathrm{d}x_1\right) - (c_\mathrm{r}\Delta w)^2\frac{1}{24}\mathrm{d}x_1\mathrm{d}x_2. \qquad (20)$$

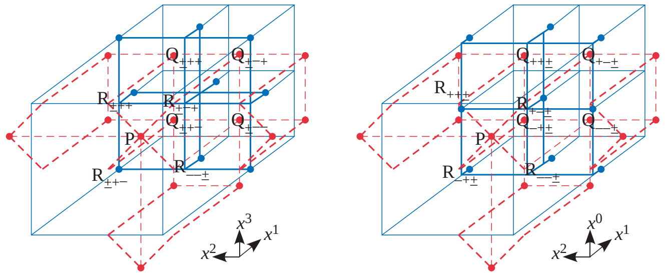

Fig. 6. 4D staircase-type subgrid connection.

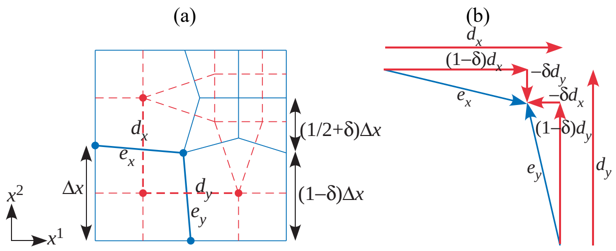

Fig. 7. Corner correction

D. *Corner correction*

Ref. [11] proposed a symmetric correction for the corner variables (Fig. 7), where the orthogonality (6) may not be satisfied. The electromotive forces (e_x, e_y) and the electric fluxes (d_x, d_y) are given by the first and second of (5), respectively. When the parameter δ ≠ 0, the face for e_x (or e_y) is not orthogonal to the face for d_x (d_y). Based on the vectorial relation [Fig. 7(b)], a symmetric correction is appropriate:

$$\begin{bmatrix} e_x \\ e_y \end{bmatrix} = \frac{Z\Delta w}{\Delta x}\begin{bmatrix} 1-\delta' & -\delta' \\ -\delta' & 1-\delta' \end{bmatrix}\begin{bmatrix} d_x \\ d_y \end{bmatrix}, \qquad (21)$$

having no asymmetry arising in the impedance matrix. Because the face for e_x (e_y) is slanted along the x^0-direction (Fig. 5), δ' is given by $\delta + (c_\mathrm{r}\Delta w)^2/(12\Delta x)$ for the straight-type grid. The magnetic variables at the corners are similarly corrected symmetrically,

$$\begin{bmatrix} h_x \\ h_y \end{bmatrix} = \frac{\Delta w}{Z\Delta x}\begin{bmatrix} 1-\delta'' & \delta'' \\ \delta'' & 1-\delta'' \end{bmatrix}^{-1}\begin{bmatrix} b_x \\ b_y \end{bmatrix}, \qquad (22)$$

where (b_x, b_y) and (h_x, h_y) are the magnetic fluxes and magneto motive forces and δ''= δ − Δx/12. An eigenvalue analysis [11] showed that the 4D subgrid schemes for the straight and staircase types are conditionally stable with and without the symmetric correction.

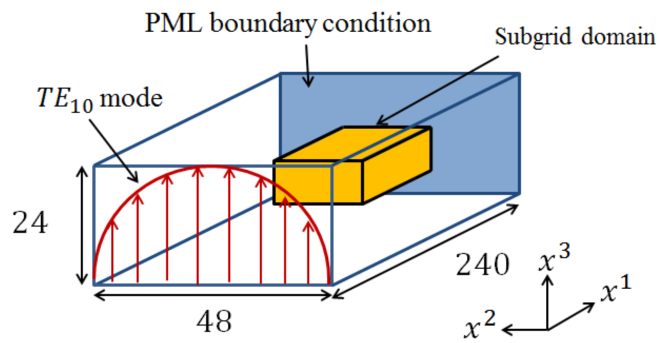

Fig. 8. Schematic of the waveguide.

V. NUMERICAL ASSESSMENT

The waveguide (Fig. 8) is used to evaluate the 4D staircase-type subgrid scheme with corner corrections with δ = 0.12. For simplicity, the permittivity and permeability are set uniformly to unity by normalization in the same way as in IV.A. The normalized spatial domain size is $240 \times 48 \times 24$ including a subgrid domain of $120 \leq x^1 \leq 180$, $12 \leq x^2 \leq 36$, and $6 \leq x^3 \leq 18$. The inlet field values are given to excite the TE_{10} mode. The PML absorbing boundary condition is applied at the exit.

Figs. 9(a) and (b) shows the propagation of the incident wave E_3^{in} and B_2^{in}, respectively, at $x^0 = 240$, which is simulated with $(\Delta x, \Delta w) = (1, 0.4)$; the normalized frequency is 0.05 measured by the normalized coordinate x^0. Fig. 9(c) depicts the propagation of the reflected wave B_2^{re} at $x^0 = 240$, which is unphysically yielded by the subgrid connection at $x^1 = 120$. For comparison, Fig. 9(d) shows the reflected wave obtained by the subgrid scheme based on the spatial FI method given in [6]. The space-time FI subgrid reduces the maximal $|B_2^{\mathrm{re}}|$ by a factor of 0.4 compared with the spatial FI scheme.

To evaluate theses unphysical reflections, the Poynting vectors of the incidence and reflected waves are averaged along the x^2-x^3 cross-section; these vectors are denoted by $p^{\mathrm{in}}(x^1)$ and $p^{\mathrm{re}}(x^1)$, respectively and their maximal absolute values along the x^1-direction are $p^{\mathrm{in}}_{\mathrm{mx}}$ and $p^{\mathrm{re}}_{\mathrm{mx}}$. Fig. 10 compares the square root of $p^{\mathrm{re}}_{\mathrm{mx}} / p^{\mathrm{in}}_{\mathrm{mx}}$ obtained by the spatial FI subgrid scheme and the proposed space-time FI subgrid, where $(\Delta x, \Delta w) = (2, 0.8), (1, 0.4), (0.5, 0.2)$ and three subgrid domains below are examined:

(a) [120, 180] × [12, 36] × [6, 18],
(b) [140, 200] × [16, 40] × [6, 18],
(c) [140, 200] × [12, 36] × [8, 20].

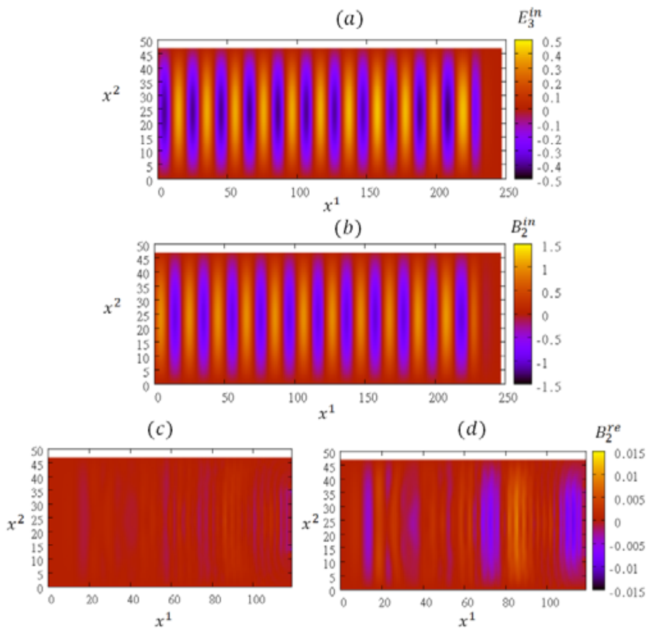

Fig. 9. Propagation of E_3 and B_2. (a) Incident wave E_3^{in}. (b) Incident wave B_2^{in}. (c) Reflected wave B_2^{re} obtained employing staircase-type subgrid. (d) Reflected wave B_2^{re} obtained employing special FI subgrid in [6].

For comparison, Fig. 10 also shows the result given by the space-time FI subgrid without the corner correction and with δ = 0.08. The space-time FI subgrid scheme yields smaller unphysical wave reflections than the spatial FI subgrid. The corner correction improves the accuracy.

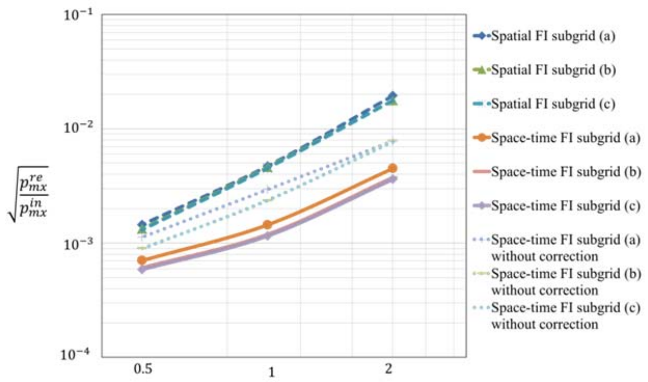

Fig. 10. The magnitude of reflected wave normalized by the incidence wave.

VI. CONCLUSION

The PML absorbing boundary condition is introduced in a natural manner into the space-time FI method. The 4D space-time subgrid connections of the straight and staircase types are discussed in the framework of the Hodge dual grid. The space-time FI method using the staircase-type subgrid reduces unphysical wave reflection compared with the conventional subgrid based on the spatial FI method.

REFERENCES

[1] Y. Hao and R. Mittra, "FDTD modeling of metamaterials: Theory and applications," *Artech House*, 2008.
[2] A. Taflove and S. C. Hagness, "Computational electrodynamics: The finite difference time-domain method," *Artech House*, 2005.
[3] T. Weiland, "Time domain electromagnetic field computation with finite difference methods," *Int. J. Numer. Model.*, vol.9, pp.295-319, Jul. 1996.
[4] I. E. Lager, E. Tonti, A.T. de Hoop, G. Mur, and M. Marrone, "Finite formulation and domain-integrated field relations in electromagnetics—a synthesis," *IEEE Trans. Magn.*, vol. 39, pp. 1199–1202, May 2003.
[5] L. Codecasa, and M. Politi, "Explicit, consistent, and conditionally stable extension of FD-TD to tetrahedral grids by FIT," *IEEE Trans. Magn.*, vol. 44, pp. 1258–1261, Jun. 2008.
[6] P. Thoma and T. Weiland, "A consistent subgridding scheme for the finite difference time domain method," *Int. J. Numer. Model.*, vol. 9, pp. 359–374, Sept. 1996.
[7] T. Matsuo, "Space-time finite integration method for electromagnetic field computation," *IEEE Trans. Magn.*, vol. 47, pp. 1530-1533, May. 2011.
[8] J. Kawahara, T. Mifune, and T. Matsuo, "Geometrical formulation of a 3D space-Time finite integration method, *IEEE Trans. Magn.*, vol. 49, pp.1693-1696, May 2013.
[9] T. Matsuo, T. Shimoi, J. Kawahara, and T. Mifune, "A simple subgrid scheme using space-time finite integration method," *IEEE Trans. Magn.*, vol. 51, 7201904, Mar. 2015.
[10] J.-P. Berenger, "A perfectly matched layer for the absorption of electromagnetic waves," *J. Comput. Phys.*, vol. 114, pp. 185-200, Oct. 1994.
[11] T. Matsuo, J. Kawahara, T. Shimoi, and T. Mifune, "Stability analysis of space-Time finite integration schemes, *Compel* (to appear).